Research Square

Preprints are preliminary reports that have not undergone peer review.
They should not be considered conclusive, used to inform clinical practice,
or referenced by the media as validated information.

A Comparative Study of Advanced DCE Tracer Kinetic Models for IDH1 Genotyping and Progression-Free Survival Prediction in Gliomas

Yujie Ding
Tongji Hospital
Nanxi Shen
Tongji Hospital
Yuanhao Li
Tongji Hospital
Hongquan Zhu
Tongji Hospital
Yufei Liu
Tongji Hospital
Shaolong Wu
Tongji Hospital
Yizhou Wan
Tongji Hospital
Li Li
Tongji Hospital
Wenzhen Zhu
zhuwenzhen8612@163.com

Tongji Hospital

Research Article

Keywords: Glioma, Isocitrate Dehydrogenase, Dynamic Contrast-Enhanced MRI, Prognosis, Tracer Kinetic Model

Posted Date: November 19th, 2026

DOI: https://doi.org/10.21203/rs.3.rs-10427848/v1

License: This work is licensed under a Creative Commons Attribution 4.0 International License. Read Full License

Additional Declarations: No competing interests reported.

Abstract

Objective

To compare quantitative dynamic contrast-enhanced (qDCE)-MRI tracer kinetic models for differentiating IDH1 subtypes and to assess their value in predicting progression-free survival (PFS) in high-grade gliomas (HGGs).

Materials and Methods

This retrospective study analyzed preoperative qDCE-MRI from 80 patients with pathologically confirmed glioma. Quantitative parameters from TOFTS, EXTOFTS, ATH, BRIX, DP, and QTM models were computed. ROC analysis was used to assess IDH1 prediction. Cox proportional hazards regression was used to evaluate PFS prediction in 34 HGGs.

Results

The distributed parameter (DP) model's cerebral blood volume (CBV) was the best single predictor of IDH1 status (AUC = 0.846). A combined model incorporating DP-CBV, QTM-derived fluid flow velocity, and tumor location achieved the highest diagnostic performance, with an apparent AUC of 0.909, a bootstrap .632 + AUC of 0.898, and a stratified 5-fold cross-validation AUC of 0.881 ± 0.011. The DP model's permeability-surface area product (PS) was an independent predictor of poor PFS in HGG (HR = 2.22; $P < 0.001$). The prognostic model combining DP parameters and clinical factors had the highest apparent C-index (0.870), significantly outperforming a clinical-only model. Correlations were observed between key parameters (e.g., DP-CBV/PS) and angiogenesis/proliferation markers (VEGF, CD31, Ki-67; $P < 0.05$).

Conclusion

Advanced qDCE-MRI models, particularly the DP model, effectively distinguish IDH1 molecular subtypes and predict PFS in HGG. DP-CBV is the optimal single imaging biomarker for IDH1 genotyping, further enhanced by combining with QTM-u and tumor location. In the exploratory PFS analysis, DP-PS is an independent prognostic imaging marker for poor PFS. Integration of these qDCE-MRI parameters with clinical assessment may enhance diagnostic and prognostic stratification for personalized glioma management.

Introduction

Gliomas are the most prevalent primary brain tumors, with high-grade gliomas (HGG) comprising approximately 60% of these lesions[1]. The 2021 World Health Organization (WHO) Classification of Central Nervous System (CNS) Tumors established the integration of molecular markers into diagnostic criteria, fundamentally altering how gliomas are diagnosed and managed[2]. Within this molecular framework, isocitrate dehydrogenase (IDH) mutation status is a key diagnostic and prognostic factor. IDH mutant gliomas exhibit a less aggressive clinical course, better treatment response, and longer progression-free survival (PFS) than IDH wild-type tumors[3]. Several clinical and conventional MRI factors such as patient age, sex, and tumor location also play a pivotal role in prognostic assessment[4–6]. Non-invasive preoperative determination of IDH status is therefore paramount for accurate diagnosis and prognostic stratification, circumventing the limitations of invasive biopsy.

Quantitative dynamic contrast-enhanced magnetic resonance imaging (qDCE-MRI) serves as a non-invasive imaging modality that offers valuable in vivo insights into the physiological and metabolic states of tissues[7]. It is particularly effective in assessing microvascular characteristics, such as vascular density and endothelial permeability [8, 9]. QDCE-MRI data can be achieved by applying tracer kinetic (TK) models to describe contrast agent dynamics. However, the

traditional approaches, such as the TOFTS and Extended Tofts (EXTOFTS) models, rely on simplified assumptions and yield parameters like the volume transfer constant (K_{trans}) that conflate the distinct biophysical processes of blood flow and vessel wall permeability[10]. This inherent ambiguity has contributed to contradictory reports on the diagnostic and prognostic value of K_{trans} and other conventional parameters[11–14].

Recent advances in TK modeling have introduced more advanced approaches, such as the distributed parameter (DP) model[15], BRIX's conventional two-compartment (BRIX) model[8], and the adiabatic tissue homogeneity (ATH) model[16]. These advanced models aim to improve the accuracy of capturing contrast agent dynamics within tissue microenvironment by separately modeling blood flow and endothelial permeability, which have shown promising applications in assessing molecular characteristics and monitoring treatment responses across various tumors, including gliomas[17–19]. Additionally, the quantitative transport mapping (QTM) method has emerged as a novel technique, allowing for the estimation of perfusion parameters without the need for an arterial input function (AIF)[20–22].

However, the choice of kinetic model is not arbitrary, different physiological assumptions yield varying parameter estimations, complicating standardization. To date, there are no study has systematically compared multiple TK models for IDH genotyping or integrated them with clinical and molecular factors for survival prediction. This limits the identification of optimal clinically relevant DCE-MRI models and parameters for these key clinical questions under the 2021 WHO classification.

This study aims to (1) compare the diagnostic performance of multiple DCE-MRI models (TOFTS, EXTOFTS, ATH, BRIX, DP, and QTM) and their derived parameters in distinguishing glioma IDH1 molecular subtypes, and (2) assess their ability to predict progression-free survival in high-grade gliomas. The study also correlates imaging parameters with immunohistochemical markers of angiogenesis and proliferation (VEGF, CD31, Ki-67), strengthening their physiological basis.

Materials and Methods

Patient Population

This retrospective study was approved by our hospital's Ethics Committee (IRB number: TJ-IRB202412200), and written informed consent was obtained from all subjects. Consecutive patients with pathologically confirmed primary gliomas and known IDH1 genotype who underwent preoperative DCE-MRI between April 2017 and December 2022 were included. Patients younger than 18 years, with purely cystic lesions, or with poor image quality were excluded. Finally, 80 patients were enrolled, and 34 HGG patients were followed up for two years after surgery. The flowchart for participant selection criteria is shown in Fig. 1.

Image Data Acquisition

MRI was performed on a 3T system (Discovery MR750, GE Healthcare) using a 32-channel head coil. Pre-contrast imaging included T1 fluid-attenuated inversion recovery (T1-FLAIR), T2 fast spin echo (T2-FSE), T2-FLAIR, diffusion weighted imaging, and T1 mapping acquired with five flip angles (3°, 6°, 9°, 12°, and 15°). DCE-MRI was performed after intravenous administration of a contrast agent (Gd, Omniscan, 0.1 mmol/kg). Finally, a routine late contrast-enhanced T1-weighted (CE-T1W) scan was acquired. Detailed scan parameters are listed in Appendix S1.

Histological Examination

Available histopathological and molecular information was reviewed in the context of the 2021 WHO CNS Classification. The IDH1 genotype was evaluated using immunohistochemical staining or next-generation sequencing. The Ki-67 labeling

index (LI), VEGF, and CD31 expression were detected using standard immunohistochemical methods. Detailed evaluation methods are provided in Appendix S2.

Image Processing and Regions of Interest Analysis

The DCE image processing was performed using commercially available software (MItalytics, FITPU Healthcare, Singapore) for five TK models: TOFTS [reverse reflux rate constant (K_{ep}; min^{-1}), K_{trans} (min^{-1}), and extravascular extracellular volume (V_e; mL/mL)], EXTOFTS [K_{ep}, K_{trans}, V_e, and blood volume (V_p; mL/mL)], ATH model [cerebral blood flow (CBF, mL/min/ mL), cerebral blood volume (CBV; mL/mL), extraction fraction (E; %), K_e, mean transit time (MTT; s), permeability-surface area product (PS; mL/min/mL), and V_e], BRIX model [CBF, CBV, E, MTT, PS, and V_e], and DP model [CBF, CBV, E, MTT, PS, and V_e], generating a total of 26 qDCE parameters. The vascular input function (VIF) was obtained from the superior sagittal sinus. In addition, we used the QTM method to calculate the fluid flow velocity (|u|; mm/s). The mathematical equations used for each model are provided in Appendix S3.

Two radiologists (3 and 12 years of experience) independently delineated the tumor regions of interest (ROIs) on original DCE-MRI referring to T1-FLAIR, T2-FSE, T2-FLIAIR, and CE-T1. The ROIs should avoid the areas of hemorrhage, calcification, oedema, necrosis, cystic lesions and blood vessels. All qDCE parameters were normalized to contralateral white matter.

Statistical Analysis

The statistical analysis was performed with SPSS (version 26.0, IBM Corporation) and R software (version 4.4.1). Intraclass Correlation Coefficient (ICC) was used to assess inter-observer reliability. Group comparisons used *t*-tests (for normally distributed data) or Mann–Whitney *U* tests (for non-normally distributed data). Receiver operating characteristic (ROC) curves were employed to calculate the area under the curve (AUC), sensitivity, specificity and cut-off value. Spearman correlation analysis was performed to evaluate the associations between qDCE parameters, Ki-67 LI, and vascular-related markers. Stepwise logistic regression (LR) was used to construct the TOFTS, EXTOFTS, ATH, BRIX, DP, QTM, and combined models; AUCs were compared by the DeLong test. Calibration of the LR models was assessed using calibration curves and Brier scores. The Brier score quantifies overall prediction error by measuring the mean squared difference between predicted probabilities and observed outcomes. Clinical utility was evaluated using decision curve analysis (DCA), which estimates the net benefit of the model across a range of threshold probabilities. Cox proportional hazards (PH) models assessed predictors of PFS, with C-indices compared between models. Model performance was internally validated using bootstrap .632 + resampling with 2000 iterations and repeated stratified 5-fold cross-validation with 50 repeats. False discovery rate (FDR, Benjamini-Hochberg method) was applied for multiple comparisons, and $P < 0.05$ was considered statistically significant.

Results

Patient Characteristics

The baseline characteristics of all participants are summarized in Table 1. Significant differences ($P < 0.05$) were observed between the IDH1 mutant and wild-type glioma groups for age, necrosis or cystic changes, edema, tumor location, enhancement quality and Ki-67 expression. Figure 2 presents the DCE-MR images, quantitative parameter maps derived from the DP model, and the corresponding immunohistochemical staining (Ki-67, VEGF, and CD31) in representative cases of IDH1 mutant and IDH1 wild-type gliomas.

Table 1
Patient Characteristics

Variable	IDH1 mutant (n = 38)	IDH1 wild-type (n = 42)	*P* value
Age (years)	44.92 ± 10.53	52.40 ± 10.44	0.001
Sex			0.796
Male	21(55.26%)	22(52.38%)	
Female	17(44.74%)	20(47.62%)	
Necrosis or cysts			0.026
Present	27(71.05%)	38(90.48%)	
Absent	11(28.95%)	4(9.52%)	
Hemorrhage			0.249
Present	7(18.42%)	4(9.52%)	
Absent	31(81.58%)	38(90.48%)	
Edema			0.003
Present	24(63.16%)	38(90.48%)	
Absent	14(36.84%)	4(9.52%)	
Tumor borders			0.305
Well-defined	25(65.79%)	32(76.19%)	
Poorly-defined	13(34.21%)	10(23.81%)	
Tumor location category			< 0.001
Frontal or insula	33(86.84%)	21(50.00%)	
Others	5(13.16%)	21(50.00%)	
Enhancement Quality			< 0.001
Marked Enhancement	7(18.42%)	32(76.19%)	
Mild Enhancement	23(60.53%)	6(14.29%)	
No Enhancement	8(21.05%)	4(9.52%)	
Ki-67 Expression			< 0.001
Low Ki-67 (LI < 10)	20(52.63%)	4(9.52%)	
High Ki-67 (LI ≥ 10)	17(44.74%)	37(88.10%)	
Missing	1(2.63%)	1(2.38%)	

Age is shown as mean ± standard deviation. IDH1, IDH1, isocitrate dehydrogenase 1; LI, labeling index.

The interobserver reproducibility was good to excellent for all qDCE parameters (ICCs: 0.877–0.983) (Table S1).

Predictability of IDH1 Mutation Status

Table 2 presents a comparison of qDCE parameters between IDH1 mutant and wild-type gliomas. Significant differences ($P < 0.05$) were found between IDH1 mutant and wild-type gliomas in all qDCE parameters except for the TOFTS-K_{ep} ($P = 0.401$). Figure 3a shows the group differences of the top six qDCE parameters between IDH1 mutant and wild-type gliomas, demonstrating consistently higher values of DP-CBV, DP-MTT, ATH-CBF, ATH-CBV, EXTOFTS-V_p, and DP-PS in IDH1 wild-type gliomas than in IDH1 mutant gliomas. The results of the ROC analysis (Table S2, Fig. 3b) indicated that V_e (AUC = 0.805), V_p (AUC = 0.808), CBF (AUC = 0.826), CBV (AUC = 0.787), and u (AUC = 0.796) achieved the best discriminative performance in the TOFTS, EXTOFTS, ATH, BRIX, and QTM models, respectively. Notably, the DP-CBV (AUC = 0.846) achieved the highest discriminative performance among the individual qDCE parameters, with 81.58% sensitivity and 76.19% specificity.

Table 2
Quantitative DCE parameters in IDH1 mutant and wild-type gliomas

Parameters	IDH1 mutant	IDH1 wild-type	*P* value*
TOFTS			
K_{ep}	0.29 (0.14, 0.55)	0.24 (0.07, 0.63)	0.401
K_{trans}	1.01 (0.29, 2.33)	2.99 (0.78, 8.96)	0.004
V_e	0.75 (0.31, 1.59)	5.92 (2.15, 9.25)	< 0.001
EXTOFTS			
K_{ep}	1.51 (0.60, 3.73)	0.43 (0.20, 2.09)	0.013
K_{trans}	2.06 (1.17, 4.77)	4.93 (3.11, 9.10)	0.001
V_e	0.66 (0.39, 1.58)	1.43 (0.57, 4.58)	0.015
V_P	2.50 (1.41, 4.67)	7.18 (4.23, 11.91)	< 0.001
ATH			
CBF	2.33 (1.40, 3.23)	4.67 (3.36, 6.46)	< 0.001
CBV	3.26 (1.93, 4.34)	8.12 (4.48, 12.20)	< 0.001
E	0.81 (0.43, 1.73)	1.35 (0.81, 2.65)	0.013
K_e	0.99 (0.61, 1.23)	0.32 (0.28, 0.65)	< 0.001
MTT	1.39 (1.02, 1.84)	1.71 (1.20, 3.40)	0.036
PS	0.28 (0.09, 0.59)	0.81 (0.37, 1.74)	< 0.001
V_e	2.67 (0.58, 6.42)	9.23 (1.84, 27.63)	0.006
BRIX			
CBF	1.76 (1.34, 2.35)	3.01 (1.99, 4.47)	< 0.001
CBV	5.14 (1.44, 11.76)	17.26 (7.26, 50.18)	< 0.001
E	2.29 (1.07, 7.73)	8.19 (2.29, 17.14)	0.043
MTT	1.80 (0.71, 4.39)	6.68 (2.43, 10.64)	< 0.001
PS	0.62 (0.30, 2.01)	2.94 (0.72, 7.41)	0.003
V_e	5.18 (1.39, 15.47)	20.78 (2.44, 99.22)	0.013
DP			
CBF	1.61 (1.19, 1.98)	2.47 (1.88, 3.19)	< 0.001
CBV	2.71 (1.69, 3.72)	7.06 (4.19, 11.72)	< 0.001
E	1.94 (0.66, 5.15)	8.68 (3.81, 18.01)	< 0.001

Each parameter is presented as median (interquartile range). *P* value*, corrected for multiple comparisons. DCE, dynamic contrast-enhanced; IDH1, isocitrate dehydrogenase 1; EXTOFTS, Extended Tofts; ATH, adiabatic tissue homogeneity; BRIX, BRIX's conventional two-compartment; DP, distributed parameter; QTM, quantitative transport mapping.

Parameters	IDH1 mutant	IDH1 wild-type	*P* value*
MTT	1.50 (1.18, 2.31)	3.61 (2.02, 4.98)	< 0.001
PS	0.35 (0.15, 1.22)	2.52 (0.78, 5.41)	< 0.001
V_e	2.83 (0.46, 7.69)	6.37 (2.23, 30.74)	0.021
QTM			
u	5.78(3.55, 10.62)	21.66(11.78, 42.94)	< 0.001

Each parameter is presented as median (interquartile range). *P* value*, corrected for multiple comparisons. DCE, dynamic contrast-enhanced; IDH1, isocitrate dehydrogenase 1; EXTOFTS, Extended Tofts; ATH, adiabatic tissue homogeneity; BRIX, BRIX's conventional two-compartment; DP, distributed parameter; QTM, quantitative transport mapping.

The multivariate stepwise LR analysis revealed that the DP model including CBV (OR: 0.74, 95% CI [0.59, 0.93], *P* = 0.009) and PS (OR: 0.76, 95% CI [0.53, 1.10], *P* = 0.148), achieved the highest apparent discriminative performance among the individual DCE models, with an AUC of 0.854 (95% CI: 0.773, 0.935), a bootstrap .632 + AUC of 0.847, and a stratified 5-fold cross-validation AUC of 0.825 ± 0.010. The combined model, incorporating DP-CBV (OR, 0.74; 95% CI: 0.59, 0.91; *P* = 0.006), QTM-u (OR, 0.95; 95% CI: 0.89, 1.00; *P* = 0.044), and tumor location category (OR, 7.71; 95% CI: 1.89, 31.40; *P* = 0.004), further improved the apparent AUC to 0.909 (95% CI: 0.845, 0.973), with a bootstrap .632 + AUC of 0.898 and a stratified 5-fold cross-validation AUC of 0.881 ± 0.011 (Table 3, Fig. 4). In addition, the combined model showed good calibration with the lowest Brier score among all models (0.137) and favorable net benefit on decision curve analysis for IDH genotyping (Fig. 4). However, the improvements in AUC were not statistically significant (*P* > 0.05) (Table S3).

Table 3
Multivariate logistic regression models for IDH1 genotyping in gliomas

Model	Parameters	OR (95%CI)	*P* value	AUC (95%CI)	Bootstrap .632 + AUC	5-fold cross-validation AUC*	Sensitivity (%)	Specificity (%)	
TOFTS		K_{trans}	0.98 (0.97, 1.00)	0.022	0.841 (0.752, 0.931)	0.834	0.814 ± 0.011	68.42	90.48
		V_e	0.76 (0.66, 0.89)	< 0.001					
EXTOFTS		V_p	0.72 (0.61, 0.86)	< 0.001	0.808 (0.705, 0.888)	0.806	0.792 ± 0.008	84.21	66.67
ATH		CBF	0.57 (0.35, 0.92)	0.020	0.843 (0.756, 0.929)	0.838	0.822 ± 0.008	84.21	76.19
		CBV	0.87 (0.71, 1.07)	0.180					
BRIX		CBV	0.87 (0.78, 0.97)	0.014	0.821 (0.732, 0.911)	0.800	0.770 ± 0.017	94.74	57.14
		MTT	1.16 (0.98, 1.37)	0.081					
		V_e	0.99 (0.98, 1.01)	0.258					
DP		CBV	0.74 (0.59, 0.93)	0.009	0.854 (0.773, 0.935)	0.847	0.825 ± 0.010	76.32	80.95
		PS	0.76 (0.53, 1.10)	0.148					
QTM		u	0.90 (0.85, 0.95)	< 0.001	0.796 (0.691, 0.878)	0.795	0.781 ± 0.008	81.58	76.19
Combined model		DP-CBV	0.74 (0.59, 0.91)	0.006	0.909 (0.845, 0.973)	0.898	0.881 ± 0.011	92.11	78.57
		QTM-u	0.95 (0.89, 1.00)	0.044					

5-fold cross-validation AUC* are presented as mean ± SD. IDH1, isocitrate dehydrogenase 1; OR, odds ratio; AUC, area under the curve; CI, confidence interval; EXTOFTS, Extended Tofts; ATH, adiabatic tissue homogeneity; BRIX, BRIX's conventional two-compartment; DP, distributed parameter; QTM, quantitative transport mapping.

Model	Parameters	OR (95%CI)	*P* value	AUC (95%CI)	Bootstrap .632 + AUC	5-fold cross-validation AUC*	Sensitivity (%)	Specificity (%)
		Tumor location category	7.71 (1.89, 31.40)	0.004				

5-fold cross-validation AUC* are presented as mean ± SD. IDH1, isocitrate dehydrogenase 1; OR, odds ratio; AUC, area under the curve; CI, confidence interval; EXTOFTS, Extended Tofts; ATH, adiabatic tissue homogeneity; BRIX, BRIX's conventional two-compartment; DP, distributed parameter; QTM, quantitative transport mapping.

Cox proportional hazards analysis on progression-free survival

Table S4 presents the baseline characteristics of 34 HGG patients with two years follow-up. Univariate Cox regression analysis revealed that the younger age, IDH1 mutation, WHO grade 3, and frontal or insula gliomas were significant predictors ($P < 0.05$) of good PFS. Furthermore, with the exception of TOFTS-K_{ep}, TOFTS-K_{trans}, EXTOFTS-K_{ep}, EXTOFTS-V_e, ATH-E, ATH-MTT, ATH-V_e, BRIX-V_e, DP-E, DP-V_e, and QTM-u, all qDCE parameters were identified as a significant predictor of the PFS of HGGs ($P < 0.05$). Notably, the higher DP-PS was identified as a significant predictor of poor PFS (HR: 2.22; 95% CI [1.43, 3.44]; $P < 0.001$) (Table S5).

Multivariable Cox regression analyses were performed based on each DCE model incorporating clinical factors, including the parameters with $P < 0.05$ in the univariable analysis. Table 4 shows the multivariable Cox regression results, indicating that the age, tumor location, TOFTS-V_e, EXTOFTS-K_{trans}, BRIX-PS, and DP-PS were the independent predictors of PFS in HGGs ($P < 0.05$). The DP model combined with clinical factors achieved the highest apparent C-index of 0.870 (95% CI: 0.788, 0.951), followed by the BRIX model (C-index = 0.863; 95% CI: 0.772, 0.953) and the EXTOFTS model (C-index = 0.851; 95% CI: 0.787, 0.915). After internal validation, the DP model maintained relatively favorable discriminative performance, with a bootstrap .632 + C-index of 0.825 and a 5-fold cross-validation C-index of 0.792 ± 0.025. The EXTOFTS and BRIX models also showed relatively preserved internally validated performance, with bootstrap .632 + C-indices of 0.826 and 0.820 and 5-fold cross-validation C-indices of 0.802 ± 0.027 and 0.782 ± 0.029, respectively (Table 4). Figure S1 illustrates the C-index comparisons across different models. Combining the DP and BRIX parameters with clinical factors significantly enhanced the predictive efficacy compared to the model solely based on clinical factors ($P = 0.015$, $P = 0.013$, respectively).

Table 4
Multivariable Cox proportional hazards regression models for predicting progression-free survival in high-grade gliomas

Model	Parameters	HR (95% CI)	*P* value	Apparent C-index(95%CI)	Bootstrap .632 + C-index	5-fold cross-validation C-index*
Clinical Factors	Age	1.11 (1.03, 1.20)	0.005	0.804 (0.706–0.903)	0.782	0.755 ± 0.021
	IDH1 status	0.26 (0.06, 1.19)	0.082			
	Tumor location category	0.26 (0.09, 0.75)	0.012			
TOFTS + Clinical Factors	Age	1.09 (1.01, 1.17)	0.030	0.808 (0.718–0.898)	0.790	0.773 ± 0.013
	Tumor location category	0.15 (0.05, 0.44)	0.001			
	TOFTS-V_e	1.99 (1.13, 3.50)	0.018			
EXTOFTS + Clinical Factors	Age	1.12 (1.02, 1.22)	0.013	0.851 (0.787–0.915)	0.826	0.802 ± 0.027
	IDH1 status	0.30 (0.07, 1.40)	0.127			
	Tumor location category	0.19 (0.06, 0.57)	0.003			
	EXTOFTS-K_{trans}	1.88 (1.18, 3.00)	0.007			
ATH + Clinical Factors	Age	1.10 (1.01, 1.20)	0.023	0.832 (0.746–0.918)	0.802	0.774 ± 0.026
	IDH1 status	0.32 (0.07, 1.51)	0.149			
	Tumor location category	0.27 (0.09, 0.78)	0.016			
	ATH-PS	1.49 (0.95, 2.33)	0.084			
BRIX + Clinical Factors	Age	1.11 (1.02, 1.22)	0.015	0.863 (0.772–0.953)	0.820	0.782 ± 0.029
	IDH1 status	0.35 (0.07, 1.69)	0.190			
	Tumor location category	0.20 (0.06, 0.63)	0.006			
	BRIX-PS	1.73 (1.15, 2.62)	0.009			

5-fold cross-validation C-index* are presented as mean ± SD. HR, hazard ratio; CI, confidence interval; IDH1, isocitrate dehydrogenase 1; EXTOFTS, Extended Tofts; ATH, adiabatic tissue homogeneity; BRIX, BRIX's conventional two-compartment; DP, distributed parameter; QTM, quantitative transport mapping.

Model	Parameters	HR (95% CI)	*P* value	Apparent C-index(95%CI)	Bootstrap .632 + C-index	5-fold cross-validation C-index*
DP + Clinical Factors	Age	1.09(0.99, 1.20)	0.085	0.870 (0.788–0.951)	0.825	0.792 ± 0.025
	Tumor location category	0.12(0.04, 0.38)	< 0.001			
	DP-MTT	1.61(0.90, 2.86)	0.108			
	DP-PS	2.09(1.10, 3.98)	0.024			

5-fold cross-validation C-index* are presented as mean ± SD. HR, hazard ratio; CI, confidence interval; IDH1, isocitrate dehydrogenase 1; EXTOFTS, Extended Tofts; ATH, adiabatic tissue homogeneity; BRIX, BRIX's conventional two-compartment; DP, distributed parameter; QTM, quantitative transport mapping.

Correlation Between Quantitative Dynamic Contrast-enhanced Parameters with Ki-67 labeling index, VEGF and CD31 Expression

Significant correlations were observed between several qDCE parameters and histopathological biomarkers, including Ki-67 LI, VEGF, and CD31 expression. Most qDCE parameters showed positive correlations with these biomarkers, whereas a few parameters (e.g., ATH-K_e, EXTOFTS-K_{ep}) exhibited negative correlations. Detailed correlation coefficients and visualized scatterplots are provided in Figs. 5 and 6 and Supplementary Figures S2-S5.

Discussion

This study investigates the performance of six distinct qDCE-MRI TK models in assessing IDH1 mutation status and predicting patient outcomes in the context of the 2021 WHO classification of gliomas. Our findings showed that nearly all qDCE parameters could be individually used to distinguishing IDH1 wild-type from mutant gliomas. Specifically, the DP model-derived CBV demonstrated the most effective single parameter for IDH1 genotyping, and a combined model incorporating DP-CBV, QTM-u, and tumor location enhanced predictive power. Importantly, this combined model maintained favorable performance after internal validation, with an apparent AUC of 0.909, a bootstrap .632 + AUC of 0.898, and a 5-fold cross-validation AUC of 0.881 ± 0.011. For prognostic assessment, a higher DP-derived PS was associated with poorer PFS in HGGs. When integrated with clinical factors, the DP model showed the highest apparent C-index among the evaluated models and retained favorable performance after internal validation. These results were substantiated by strong correlations between advanced model parameters and immunohistochemical markers of angiogenesis (VEGF, CD31) and proliferation (Ki-67), further strengthening the biological basis and clinical relevance for their imaging-based observations.

Among the multiple TK parameters, the DP-CBV parameter stood out as the most effective independent discriminator of IDH1 mutation status. The observed superiority of advanced DCE-MRI models, especially the DP model, in differentiating IDH1 wild-type from mutant gliomas is rooted in fundamental molecular and cellular differences that drive tumor angiogenesis[23]. IDH wild-type gliomas are driven by hypoxia-inducible factor 1-alpha (HIF-1α), which promotes the expression of pro-angiogenic factors like VEGF[24, 25]. Increased VEGF expression promotes the formation of a chaotic and functionally abnormal microvasculature, featuring high vessel density, enlarged vessel calibers, and poorly formed endothelial junctions, leading to increased vascular permeability. Our findings align with this biology, showing that IDH wild-type tumors exhibit significantly higher values for parameters reflecting blood volume, blood flow, and PS across multiple models. Indeed, numerous studies using conventional DCE-MRI or dynamic susceptibility contrast (DSC)-MRI,

which similarly found that IDH wild-type gliomas exhibit higher relative CBV than IDH mutant tumors[26, 27]. A recent study by Zhang et al. (2024) [28]also compared the DP and EXTOFTS models, finding they performed similarly for IDH prediction with V_e being the optimal parameter. This divergence likely stems from variations in patient cohorts, MRI acquisition protocols, or AIF selection methodologies[28].

The study's demonstration of significant positive correlations between DP-CBV/DP-PS and VEGF and CD31 expression, and between nearly all perfusion/permeability parameters and the Ki-67 proliferation index provides strong biological validation for these imaging biomarkers[29, 30]. VEGF is a key regulator of angiogenesis and promotes vascular permeability; CD31 is a well-established endothelial cell marker reflecting microvessel density, and Ki-67 is a biomarker representing the proliferation activity of tumor cells. These correlations confirm that DCE-MRI parameters are indeed quantifying critical aspects of tumor angiogenesis, vascularity, and cellular proliferation. A more nuanced finding was the significant negative correlation between the K_{ep}/K_e and VEGF. This seemingly counterintuitive result is explained by tracer kinetics: increased VEGF expression enhances vascular permeability and expands Ve, reducing the concentration gradient for contrast reflux and thus lowering K_{ep}[31]. This observation highlights the sophisticated physiological insights that can be gleaned from advanced kinetic modeling.

The classical TK model parameters like TOFTS-K_{trans} and EXTOFTS-V_e were also found to be independent predictors of IDH1 mutation status. Higher values of these parameters were observed in IDH wild-type gliomas, which is consistent with findings from previous perfusion MRI studies[32, 33]. However, the TOFTS model assumes a homogeneous, single-compartment system and uses K_{trans}, a parameter that conflates blood flow and permeability, limiting its ability to characterize complex glioma vasculature and explaining its relatively lower performance compared to advanced models[10, 34]. In contrast, advanced models such as DP, BRIX, and ATH distinguish between two modes of tracer transport within the tissue microenvironment: intravascular perfusion and the exchange between intravascular and extravascular spaces, which are quantified by blood flow and PS[35]. For example, the DP model, by separately estimating parameters like CBV (reflecting vascular density) and PS (reflecting endothelial leakiness), are particularly adept at capturing the disorganized vasculature that define these distinct molecular subtypes. Furthermore, the BRIX and ATH models, while significant in multivariate analyses, demonstrated slightly lower performance compared to the DP model in our study. The BRIX model assumes a well-mixed vascular and extravascular space, which may not fully capture the heterogeneous nature of glioma vasculature. Similarly, the ATH model assumes a uniform extravascular space, and blood flow can vary considerably within different tumor regions, further complicating the accuracy of these assessments[36]. Nonetheless, they remain valuable for distinguishing IDH mutant from wild-type gliomas.

Although existing literatures have utilized the advanced qDCE-MRI models in various diseases[17, 35, 37]; few studies have explored advanced TK models in gliomas for IDH genotyping. For example, Li et al.[19] applied the qDCE-MRI models in 55 patients with glioma and showed that superior diagnostic accuracy of the DP model compared to the TOFTS model; V_p was found to be the most distinct feature in discriminating IDH mutant from wild-type gliomas, which aligns with our study. However, this previous study focuses on the DP model and compares it only with the TOFTS model, without incorporating clinical or conventional MRI features. Our study extends this body of work by comprehensively comparing multiple kinetic models, including newer-generation approaches like DP, ATH, and QTM method, within a single cohort under the 2021 WHO classification framework. Furthermore, our combined model, leveraging parameters from two different advanced DCE models (DP-CBV, QTM-u) and the tumor location, achieved a higher AUC of 0.909, suggesting a potential synergistic benefit from integrating multi-faceted perfusion information. QTM-u quantifies the velocity of fluid flow within the tumor microenvironment without relying on an AIF, which enhances its practical clinical utility[20, 21]. Elevated QTM-u values, observed in IDH wild-type gliomas, may reflect increased hypoxia-induced angiogenesis, a finding that is consistent with observations in other malignancies[21]. Its inclusion in our best-performing combined model for IDH1 genotyping suggests that AIF-free techniques hold considerable promise for simplifying clinical workflows and

improving robustness. Additionally, tumor location serves as a potential prognostic factor, as certain regions, such as the frontal or insular lobes, are more frequently associated with IDH mutant gliomas and improved clinical outcomes[38].

Beyond diagnosis, this study also explored the prognostic value of qDCE-MRI parameters for PFS stratification in HGGs. Existing studies frequently focused primarily on traditional qDCE-MRI models such as TOFTS or EXTOFTS to explore prognosis in glioma[32, 39–41]. Some studies have applied ATH and BRIX derived DCE parameters for predicting patients' overall survival and differentiating glioma recurrence; but contradictory results across studies are obvious[11, 42, 43]. To date, there has been a paucity of data comparing the relative performance of each TK model with clinical factors for the survival prediction in gliomas. Notably, our study identified several TK model parameters, including DP-PS, BRIX-PS, EXTOFTS-K_{trans}, and TOFTS-V_e, as significant predictors of PFS in HGGs, independent of clinical and conventional MRI factors. Among the evaluated models, the DP model combined with clinical factors showed the highest apparent C-index and significantly outperformed the clinical model alone. After internal validation, the DP model maintained favorable discriminative performance, with a bootstrap .632 + C-index of 0.825 and a repeated 5-fold cross-validation C-index of 0.792 ± 0.025, compared with 0.782 and 0.755 ± 0.021 for the clinical model, respectively. The decrease from the apparent C-index to the internally validated estimates suggests a degree of optimism, which is not unexpected given the limited sample size.

Within the DP model combined with clinical factors, DP-PS was identified as an independent predictor of poor PFS. The PS reflects the permeability of the endothelial wall, which may be linked to nutrition supply to cell growth; elevated values are likely due to the excessive proliferation of tumor cells[44]. The prognostic power of DP-PS may reflect the critical role of vascular leakiness in tumor aggression; higher PS values signify a more disrupted, permeable vasculature that facilitates tumor invasion and proliferation, ultimately leading to earlier progression[19]. Compared with simplified parameters such as TOFTS-K_{trans}, the DP model accounts for heterogeneous tracer distribution and may provide a more specific estimate of vascular permeability. This may partly explain the prognostic relevance of DP-PS in HGGs. Nevertheless, given the small PFS cohort, these findings should be considered exploratory and require external validation in larger and multicenter cohorts.

Despite the promising results, this study has several limitations. First, its retrospective, single-center design and the limited size of the PFS cohort may introduce selection bias and limit generalizability. In particular, the PFS analysis included only 34 patients with HGGs and should be considered exploratory. Future large-scale, prospective, multicenter studies with sufficient follow-up are necessary to validate our findings. Second, the ROI analysis focused on enhancing or T2-hyperintense tumor while excluding necrosis and cysts, which may not fully represent tumor heterogeneity. Future studies could adopt whole-tumor histogram analysis or habitat-based imaging approaches. Third, the AIF was derived from the superior sagittal sinus, an accepted but imperfect surrogate for true arterial input that may affect perfusion quantification. The promising results from the AIF-free QTM model suggest that further exploration of such methods is warranted.

This study demonstrates that qDCE-MRI models effectively distinguish between IDH1 mutant and wild-type gliomas, with the DP model exhibiting the highest performance. The DP-CBV has shown to be the most robust biomarker for non-invasively predicting IDH1 mutation status, as validated by strong correlations with immunohistochemical angiogenesis and proliferation markers. The combined model incorporating DP-CBV and QTM-u, along with tumor location, further enhances diagnostic effectiveness for IDH1 genotyping. In the exploratory PFS analysis, higher DP-PS was associated with shorter PFS in HGGs, and the DP model combined with clinical factors showed promising prognostic performance in gliomas. These findings suggest that qDCE-MRI may provide valuable complementary information to conventional clinical assessment, potentially contributing to more precise diagnosis and outcome evaluation in glioma management.

Abbreviations

ATH
Adiabatic tissue homogeneity
AIF
Arterial input function
AUC
Area under the curve
BBB
Blood-brain barrier
BRIX
BRIX’s conventional two-compartment model
CBF
Cerebral blood flow
CBV
Cerebral blood volume
CNS
Central Nervous System
DP
Distributed parameter
DSC
Dynamic susceptibility contrast
E
Extraction fraction
HGG
High-grade gliomas
HIF-1α
Hypoxia-inducible factor 1-alpha
ICC
Intraclass Correlation Coefficient
IDH
Isocitrate dehydrogenase
K_{ep}/K_e
Reverse reflux rate constant
K_{trans}
Volume transfer constant
LI
Labeling index
MTT
Mean transit time
PFS
Progression-free survival
PS
Permeability-surface area product
QDCE
Quantitative dynamic contrast-enhanced
QTM
Quantitative transport mapping
ROC

Receiver operating characteristic
ROI
Region of interest
TK
Tracer kinetic
|u|
Fluid flow velocity
V_e
Extravascular extracellular volume
VIF
Vascular input function
V_p
Blood volume
WHO
World Health Organization

Declarations

Ethics approval and consent to participate

The study was conducted in accordance with the Declaration of Helsinki (as revised in 2013) and approved by the Institutional Review Board of Tongji Hospital affiliated with Tongji Medical College of Huazhong University of Science and Technology (ethical approval number: TJ-IRB202412200) and written informed consent was provided by all patients.

Consent for publication

Not applicable.

Competing interests

The authors declare that they have no competing interests.

Funding

This study has received funding from the National Natural Science Foundation of China (grant number U22A20354).

Author Contribution

YD, NS, and WZ conceptualized the study. YD, HZ, and SW performed data curation. YD and YhL conducted the formal analysis. WZ was responsible for funding acquisition. YD and NS performed the investigation. YD, NS, and YhL developed the methodology. WZ was responsible for project administration and provided resources. YD and NS developed the software. LL and WZ supervised the research. YfL and HZ performed validation. YW was responsible for visualization. YD and NS wrote the original draft. WZ and LL reviewed and edited the manuscript. All authors reviewed the manuscript.

Acknowledgements

Not applicable.

Data Availability

The data used to support this manuscript is reported in its entirety. More detailed raw data could not be reported because of concern for privacy and ethical issues. Readers may request to access this data for non-commercial use by reaching out to corresponding authors. Requests must explain the intended purposes for the data.

References

1. Ostrom QT, Gittleman H, Fulop J, Liu M, Blanda R, Kromer C, et al. CBTRUS Statistical Report: Primary Brain and Central Nervous System Tumors Diagnosed in the United States in 2008–2012. Neuro Oncol. 2015;17(Suppl 4):iv1–62.
2. Louis DN, Perry A, Wesseling P, Brat DJ, Cree IA, Figarella-Branger D et al. The 2021 WHO Classification of Tumors of the Central Nervous System: a summary. Neuro Oncol. 2021.
3. Beiko J, Suki D, Hess KR, Fox BD, Cheung V, Cabral M, et al. IDH1 mutant malignant astrocytomas are more amenable to surgical resection and have a survival benefit associated with maximal surgical resection. Neuro Oncol. 2014;16(1):81–91.
4. Weller M, Felsberg J, Hartmann C, Berger H, Steinbach JP, Schramm J, et al. Molecular predictors of progression-free and overall survival in patients with newly diagnosed glioblastoma: a prospective translational study of the German Glioma Network. J Clin Oncol. 2009;27(34):5743–50.
5. Kim M, Kim S, Park YW, Han K, Ahn SS, Moon JH, et al. Sex as a prognostic factor in adult-type diffuse gliomas: an integrated clinical and molecular analysis according to the 2021 WHO classification. J Neurooncol. 2022;159(3):695–703.
6. Awad AW, Karsy M, Sanai N, Spetzler R, Zhang Y, Xu Y, et al. Impact of removed tumor volume and location on patient outcome in glioblastoma. J Neurooncol. 2017;135(1):161–71.
7. Heye AK, Thrippleton MJ, Armitage PA, Valdes Hernandez MDC, Makin SD, Glatz A, et al. Tracer kinetic modelling for DCE-MRI quantification of subtle blood-brain barrier permeability. NeuroImage. 2016;125:446–55.
8. Sourbron SP, Buckley DL. Tracer kinetic modelling in MRI: estimating perfusion and capillary permeability. Phys Med Biol. 2012;57(2):R1–33.
9. Heye AK, Culling RD, Valdés Hernández Mdel C, Thrippleton MJ, Wardlaw JM. Assessment of blood-brain barrier disruption using dynamic contrast-enhanced MRI. A systematic review. Neuroimage Clin. 2014;6:262–74.
10. Koh TS, Bisdas S, Koh DM, Thng CH. Fundamentals of tracer kinetics for dynamic contrast-enhanced MRI. J Magn Reson Imaging. 2011;34(6):1262–76.
11. Larsen VA, Simonsen HJ, Law I, Larsson HB, Hansen AE. Evaluation of dynamic contrast-enhanced T1-weighted perfusion MRI in the differentiation of tumor recurrence from radiation necrosis. Neuroradiology. 2013;55(3):361–9.
12. Ahn SH, Ahn SS, Park YW, Park CJ, Lee SK. Association of dynamic susceptibility contrast- and dynamic contrast-enhanced magnetic resonance imaging parameters with molecular marker status in lower-grade gliomas: A retrospective study. Neuroradiol J. 2023;36(1):49–58.
13. Jing H, Yan X, Li J, Qin D, Zhang N, Zhang H. The Value of Dynamic Contrast-Enhanced Magnetic Resonance Imaging (DCE-MRI) in the Differentiation of Pseudoprogression and Recurrence of Intracranial Gliomas. Contrast Media Mol Imaging. 2022;2022:5680522.
14. Jensen RL, Mumert ML, Gillespie DL, Kinney AY, Schabel MC, Salzman KL. Preoperative dynamic contrast-enhanced MRI correlates with molecular markers of hypoxia and vascularity in specific areas of intratumoral microenvironment and is predictive of patient outcome. Neuro Oncol. 2014;16(2):280–91.
15. Koh TS, Cheong LH, Hou Z, Soh YC. A physiologic model of capillary-tissue exchange for dynamic contrast-enhanced imaging of tumor microcirculation. IEEE Trans Biomed Eng. 2003;50(2):159–67.

16. St Lawrence KS, Lee TY. An adiabatic approximation to the tissue homogeneity model for water exchange in the brain: I. Theoretical derivation. J Cereb Blood Flow Metab. 1998;18(12):1365–77.
17. Gao A, Wang H, Zhang X, Wang T, Chen L, Hao J, et al. Applying dynamic contrast-enhanced MRI tracer kinetic models to differentiate benign and malignant soft tissue tumors. Cancer Imaging. 2024;24(1):64.
18. Ye Z, Ning G, Li X, Koh TS, Chen H, Bai W, et al. Endometrial carcinoma: use of tracer kinetic modeling of dynamic contrast-enhanced MRI for preoperative risk assessment. Cancer Imaging. 2022;22(1):14.
19. Li Z, Zhao W, He B, Koh TS, Li Y, Zeng Y, et al. Application of Distributed Parameter Model to Assessment of Glioma IDH Mutation Status by Dynamic Contrast-Enhanced Magnetic Resonance Imaging. Contrast Media Mol Imaging. 2020;2020:8843084.
20. Zhang Q, Spincemaille P, Drotman M, Chen C, Eskreis-Winkler S, Huang W, et al. Quantitative transport mapping (QTM) for differentiating benign and malignant breast lesion: Comparison with traditional kinetics modeling and semi-quantitative enhancement curve characteristics. Magn Reson Imaging. 2022;86:86–93.
21. Huang W, Zhang Q, Wu G, Chen PP, Li J, McCabe Gillen K, et al. DCE-MRI quantitative transport mapping for noninvasively detecting hypoxia inducible factor-1alpha, epidermal growth factor receptor overexpression, and Ki-67 in nasopharyngeal carcinoma patients. Radiother Oncol. 2021;164:146–54.
22. Zhang Q, Luo X, Zhou L, Nguyen TD, Prince MR, Spincemaille P, et al. Fluid Mechanics Approach to Perfusion Quantification: Vasculature Computational Fluid Dynamics Simulation, Quantitative Transport Mapping (QTM) Analysis of Dynamics Contrast Enhanced MRI, and Application in Nonalcoholic Fatty Liver Disease Classification. IEEE Trans Biomed Eng. 2023;70(3):980–90.
23. Yan H, Parsons DW, Jin G, McLendon R, Rasheed BA, Yuan W, et al. IDH1 and IDH2 mutations in gliomas. N Engl J Med. 2009;360(8):765–73.
24. Chesnelong C, Chaumeil MM, Blough MD, Al-Najjar M, Stechishin OD, Chan JA, et al. Lactate dehydrogenase A silencing in IDH mutant gliomas. Neuro Oncol. 2014;16(5):686–95.
25. Jain R, Gutierrez J, Narang J, Scarpace L, Schultz LR, Lemke N, et al. In vivo correlation of tumor blood volume and permeability with histologic and molecular angiogenic markers in gliomas. AJNR Am J Neuroradiol. 2011;32(2):388–94.
26. Ye M, Cao Z, Zhu Z, Chen S, Zhou J, Yang H, et al. Integrating quantitative DCE-MRI parameters and radiomic features for improved IDH mutation prediction in gliomas. Front Oncol. 2025;15:1530144.
27. Yuzkan S, Karagulle M, Ozdemir MS, Mutlu S, Kocak B. Predictive Value of T2-weighted Perfusion and T1-weighted Permeability MRI Parameters in Determining IDH Mutational Status and Grade of Gliomas. Turk Neurosurg. 2024;34(6):1056–65.
28. Zhao K, Huang H, Gao E, Qi J, Chen T, Zhao G, et al. Distributed parameter model of dynamic contrast-enhanced MRI in the identification of IDH mutation, 1p19q codeletion, and tumor cell proliferation in glioma patients. Front Oncol. 2024;14:1333798.
29. Annese T, Errede M, d'Amati A, De Giorgis M, Lorusso L, Tamma R et al. Differential P-Glycoprotein/CD31 Expression as Markers of Vascular Co-Option in Primary Central Nervous System Tumors. Diagnostics (Basel). 2022;12(12).
30. Bernstock JD, Gary SE, Klinger N, Valdes PA, Ibn Essayed W, Olsen HE, et al. Standard clinical approaches and emerging modalities for glioblastoma imaging. Neurooncol Adv. 2022;4(1):vdac080.
31. Ulyte A, Katsaros VK, Liouta E, Stranjalis G, Boskos C, Papanikolaou N, et al. Prognostic value of preoperative dynamic contrast-enhanced MRI perfusion parameters for high-grade glioma patients. Neuroradiology. 2016;58(12):1197–208.
32. Zhang HW, Lyu GW, He WJ, Lei Y, Lin F, Wang MZ, et al. DSC and DCE Histogram Analyses of Glioma Biomarkers, Including IDH, MGMT, and TERT, on Differentiation and Survival. Acad Radiol. 2020;27(12):e263–71.
33. Hu Y, Chen Y, Wang J, Kang JJ, Shen DD, Jia ZZ. Non-Invasive Estimation of Glioma IDH1 Mutation and VEGF Expression by Histogram Analysis of Dynamic Contrast-Enhanced MRI. Front Oncol. 2020;10:593102.

34. Sourbron SP, Buckley DL. On the scope and interpretation of the Tofts models for DCE-MRI. Magn Reson Med. 2011;66(3):735–45.
35. Lu Y, Peng W, Song J, Chen T, Wang X, Hou Z, et al. On the potential use of dynamic contrast-enhanced (DCE) MRI parameters as radiomic features of cervical cancer. Med Phys. 2019;46(11):5098–109.
36. Vajkoczy P, Menger MD. Vascular microenvironment in gliomas. J Neurooncol. 2000;50(1–2):99–108.
37. Lee SH, Hayano K, Zhu AX, Sahani DV, Yoshida H. Dynamic Contrast-Enhanced MRI Kinetic Parameters as Prognostic Biomarkers for Prediction of Survival of Patient with Advanced Hepatocellular Carcinoma: A Pilot Comparative Study. Acad Radiol. 2015;22(11):1344–60.
38. De Leeuw BI, Van Baarsen KM, Snijders TJ, Robe P. Interrelationships between molecular subtype, anatomical location, and extent of resection in diffuse glioma: a systematic review and meta-analysis. Neurooncol Adv. 2019;1(1):vdz032.
39. Pak E, Choi KS, Choi SH, Park CK, Kim TM, Park SH, et al. Prediction of Prognosis in Glioblastoma Using Radiomics Features of Dynamic Contrast-Enhanced MRI. Korean J Radiol. 2021;22(9):1514–24.
40. Chung H, Seo H, Choi SH, Park CK, Kim TM, Park SH, et al. Cluster Analysis of DSC MRI, Dynamic Contrast-Enhanced MRI, and DWI Parameters Associated with Prognosis in Patients with Glioblastoma after Removal of the Contrast-Enhancing Component: A Preliminary Study. AJNR Am J Neuroradiol. 2022;43(11):1559–66.
41. Jo SW, Choi SH, Lee EJ, Yoo RE, Kang KM, Yun TJ, et al. Prognostic Prediction Based on Dynamic Contrast-Enhanced MRI and Dynamic Susceptibility Contrast-Enhanced MRI Parameters from Non-Enhancing, T2-High-Signal-Intensity Lesions in Patients with Glioblastoma. Korean J Radiol. 2021;22(8):1369–78.
42. Lundemann M, Munck Af Rosenschold P, Muhic A, Larsen VA, Poulsen HS, Engelholm SA, et al. Feasibility of multi-parametric PET and MRI for prediction of tumour recurrence in patients with glioblastoma. Eur J Nucl Med Mol Imaging. 2019;46(3):603–13.
43. Henriksen OM, Hansen AE, Muhic A, Marner L, Madsen K, Moller S, et al. Diagnostic yield of simultaneous dynamic contrast-enhanced magnetic resonance perfusion measurements and [(18)F]FET PET in patients with suspected recurrent anaplastic astrocytoma and glioblastoma. Eur J Nucl Med Mol Imaging. 2022;49(13):4677–91.
44. Wang X, Lin W, Mao Y, Peng W, Song J, Lu Y, et al. A Comparative Study of Two-Compartment Exchange Models for Dynamic Contrast-Enhanced MRI in Characterizing Uterine Cervical Carcinoma. Contrast Media Mol Imaging. 2019;2019:3168416.

Figures

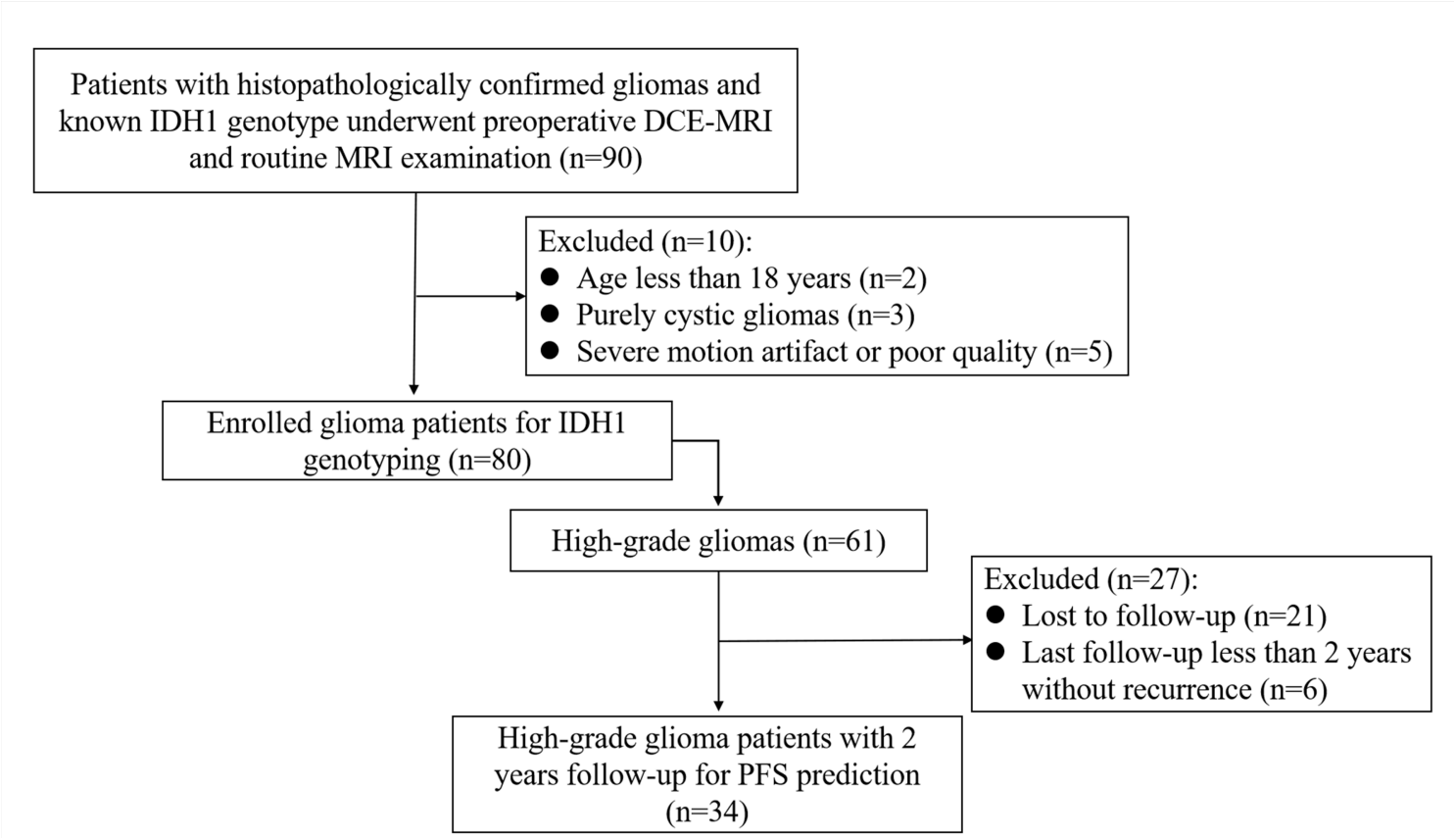


Figure 1

Flowchart showing participant selection criteria

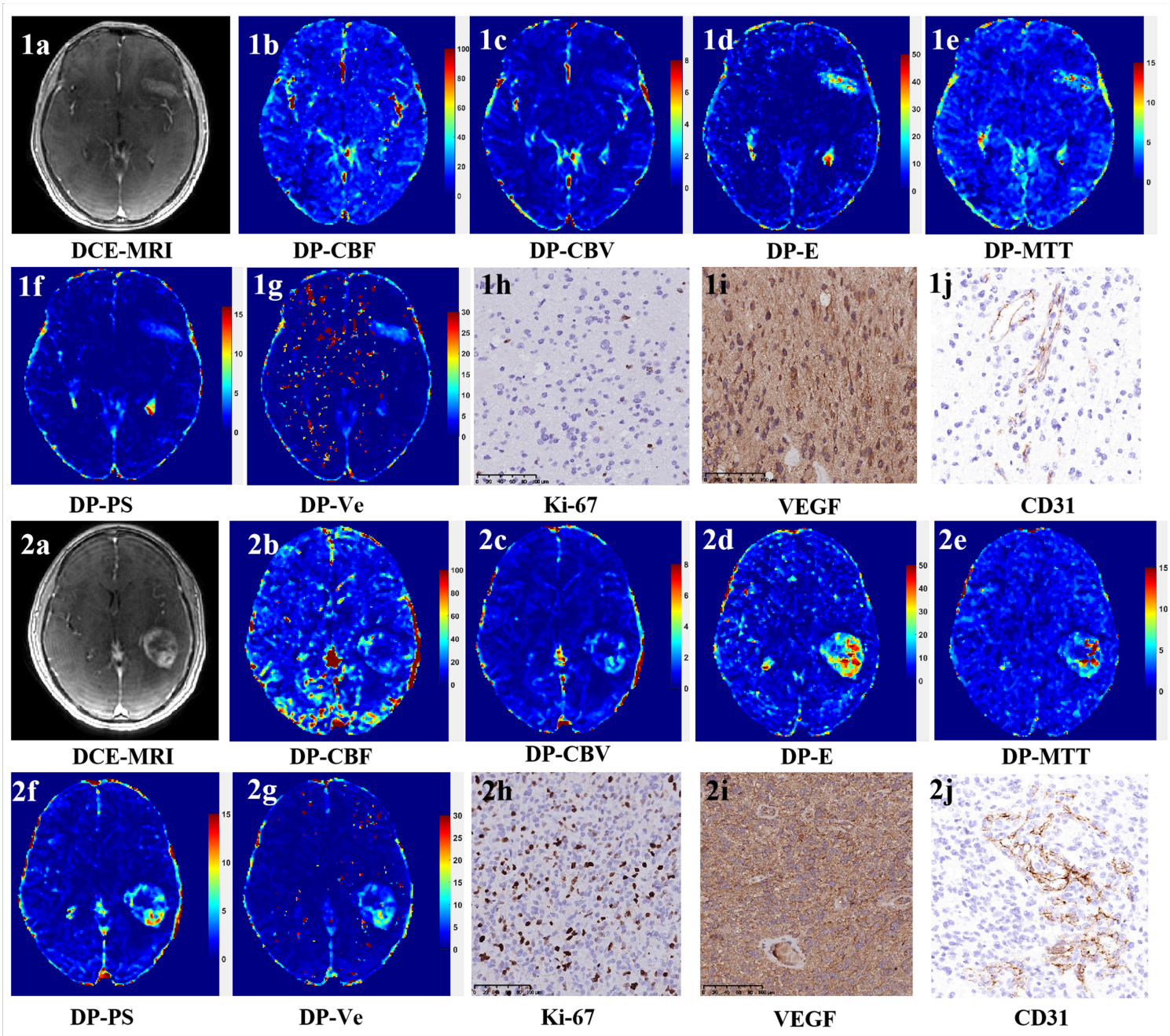


Figure 2

Representative DCE-MR images, quantitative DCE parameter maps derived from the DP model, and corresponding immunohistochemical images in patients with glioma.

(1a-1j) A patient with IDH1 mutant diffuse glioma (WHO grade 3). (1a) DCE-MR image acquired at the 40th dynamic phase; (1b-1g) parametric maps derived from the DP model, including the CBF, CBV, E, MTT, PS, and V_e; (1h-1j) immunohistochemical staining for Ki-67, VEGF, and CD31, respectively. (2a-2j) A patient with IDH1 wild-type diffuse glioma (WHO grade 4). (2a) DCE-MR image acquired at the 40th dynamic phase; (2b-2g) parametric maps derived from the DP model, including the CBF, CBV, E, MTT, PS, and V_e; (2h-2j) immunohistochemical staining for Ki-67, VEGF, and CD31, respectively. Scale bars in immunohistochemical images represent 100 μm. DCE-MRI, dynamic contrast-enhanced magnetic resonance imaging; DP, distributed parameter; IDH1, isocitrate dehydrogenase 1; CBF, cerebral blood flow; CBV, cerebral blood volume; E, extraction fraction; MTT, mean transit time; PS, permeability-surface area product; V_e, extravascular extracellular volume.

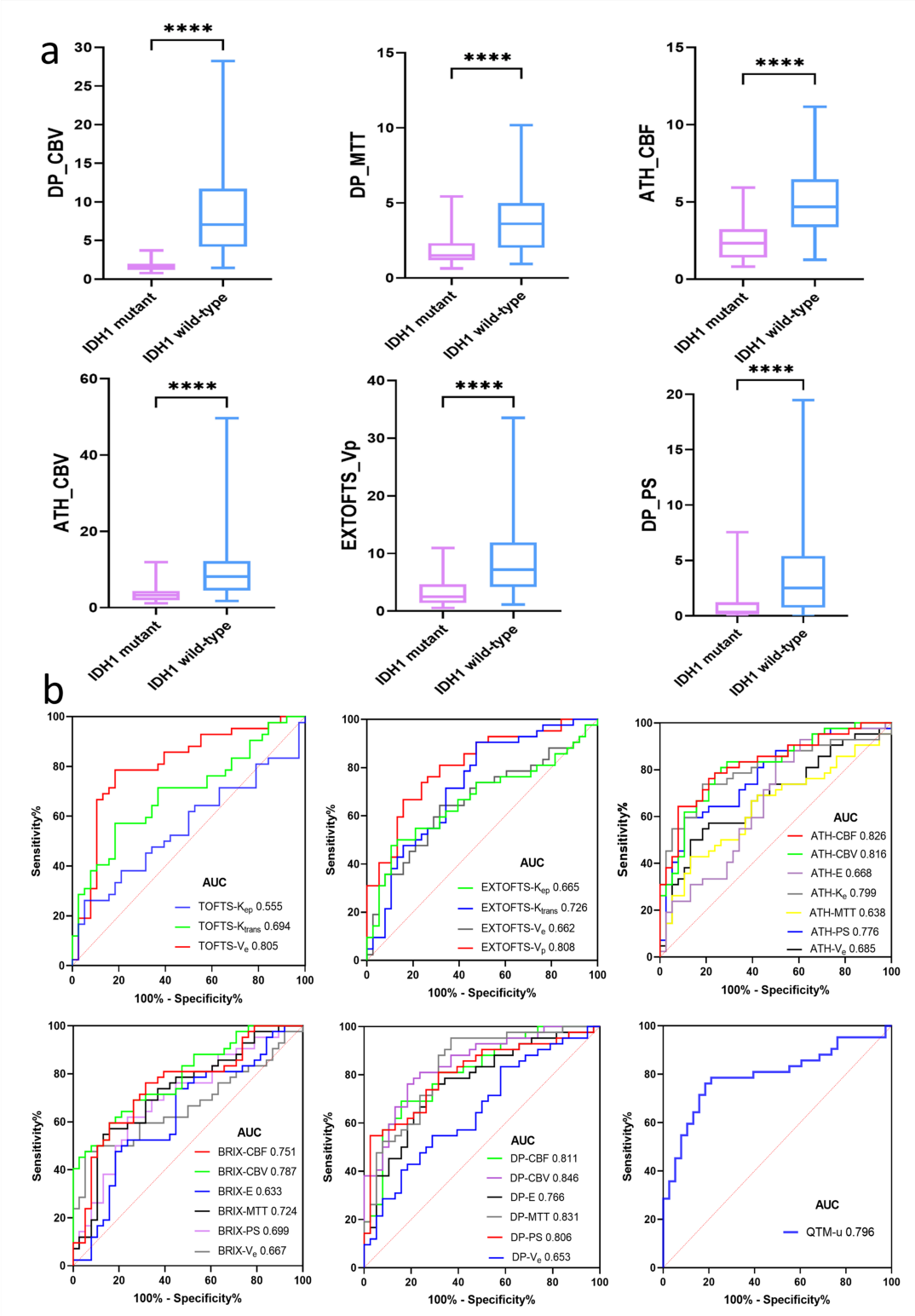


Figure 3

Box and whisker plots and receiver operating characteristic (ROC) analysis of quantitative DCE parameters for IDH1 genotyping. (a) Box and whisker plots of top six quantitative DCE parameters according to IDH1 status; (b) ROC curves of quantitative DCE parameters derived from the TOFTS, EXTOFTS, ATH, BRIX, DP, and QTM models for IDH1 genotyping. DCE, dynamic contrast-enhanced; EXTOFTS, Extended Tofts, ATH, adiabatic tissue homogeneity; BRIX, BRIX's conventional two-compartment; DP, distributed parameter; QTM, quantitative transport mapping; IDH1, isocitrate dehydrogenase 1. **** = P< 0.0001.

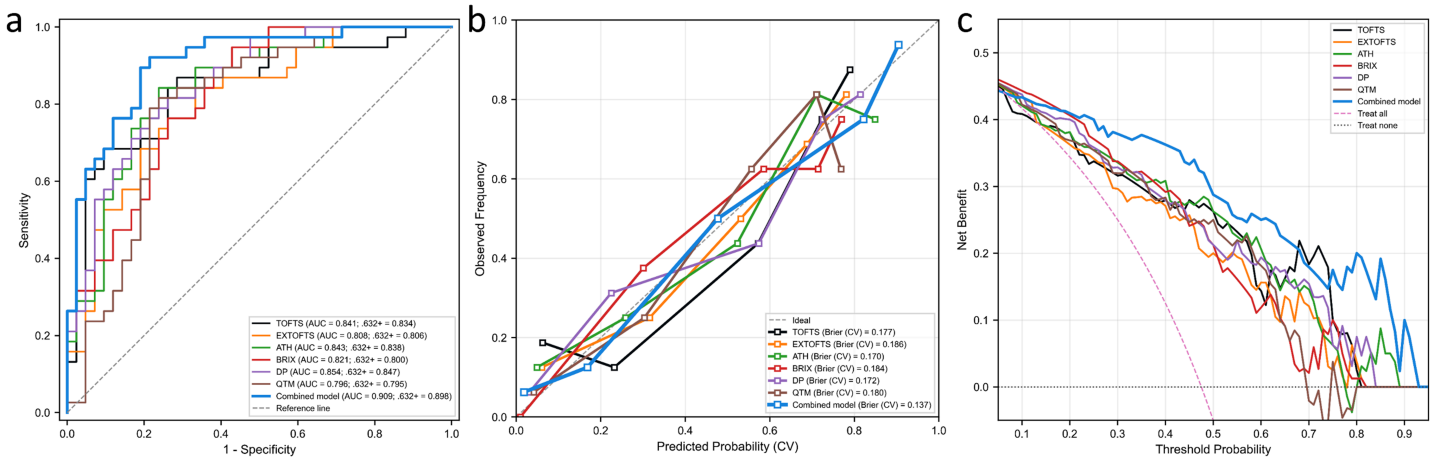


Figure 4

Logistic regression model performance for IDH1 genotyping in gliomas. (a) Receiver operating characteristic (ROC) curves, (b) calibration curves, and (c) decision curve analysis (DCA) for IDH1 genotyping. DCE, dynamic contrast-enhanced; AUC, area under the curve; EXTOFTS, Extended Tofts; ATH, adiabatic tissue homogeneity; BRIX, BRIX's conventional two-compartment; DP, distributed parameter; QTM, quantitative transport mapping; IDH1, isocitrate dehydrogenase 1.

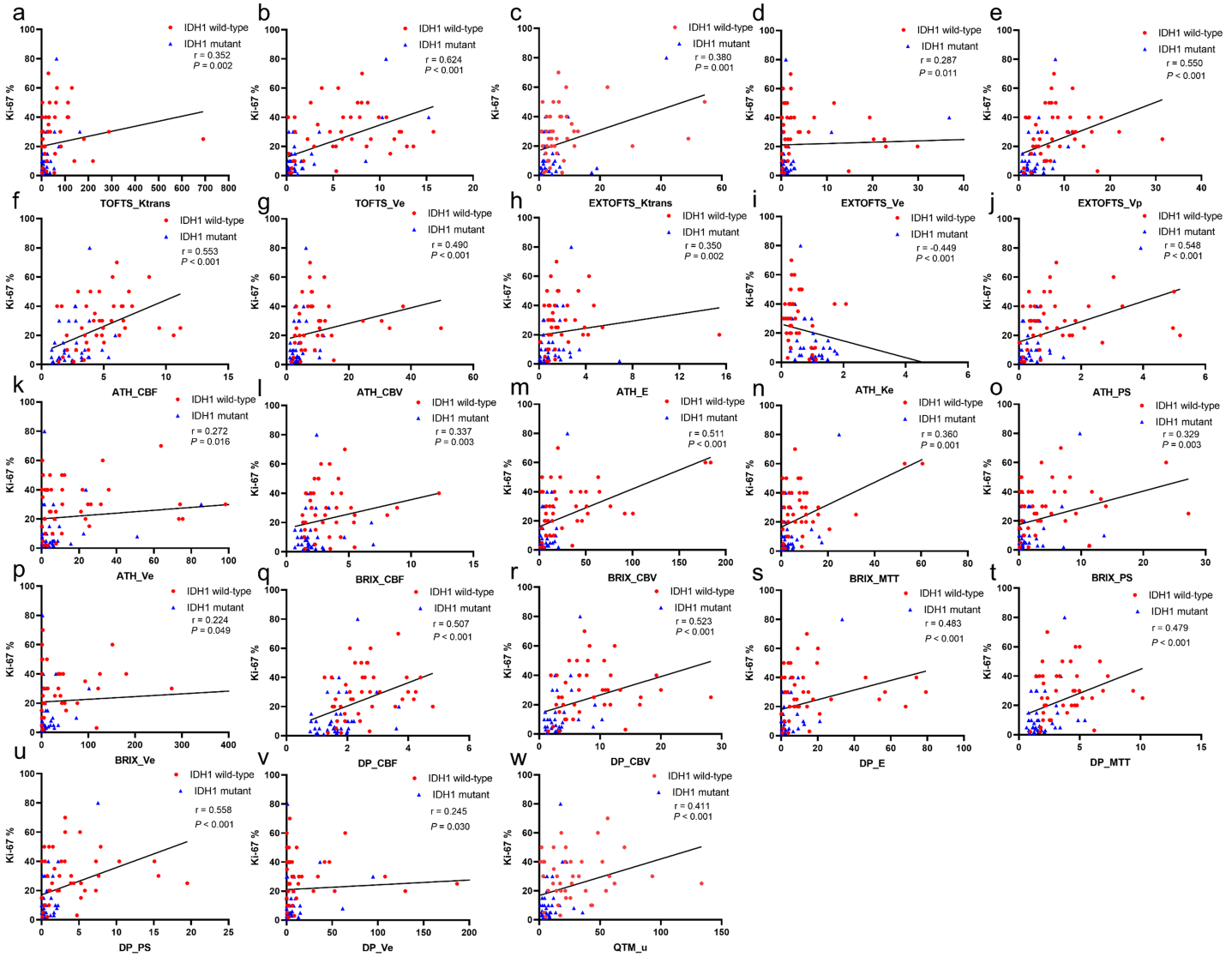


Figure 5

Quantitative DCE parameters significantly correlated with Ki-67 labeling index in glioma patients. Significant parameters were derived from (a-b) TOFTS model, (c-e) EXTOFTS model, (f-k) ATH model, (l-p) BRIX model, (q-v) DP model, and (w) QTM model. DCE, dynamic contrast-enhanced; EXTOFTS, Extended Tofts; ATH, adiabatic tissue homogeneity; BRIX, BRIX's conventional two-compartment; DP, distributed parameter; QTM, quantitative transport mapping; IDH1, isocitrate dehydrogenase 1.

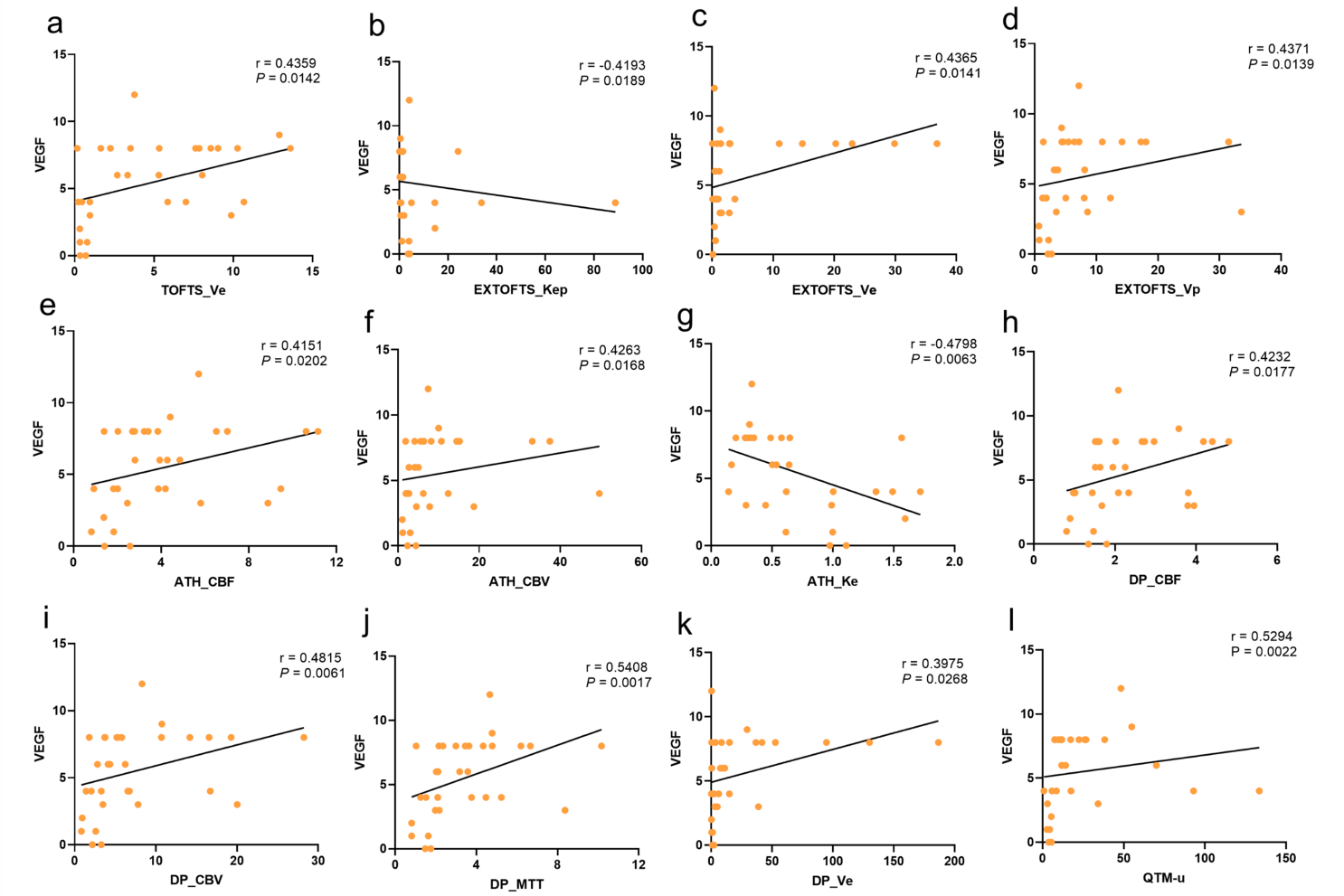


Figure 6

Quantitative DCE parameters significantly correlated with VEGF expression in glioma patients. Significant parameters were derived from (a) TOFTS model, (b-d) EXTOFTS model, (e-g) ATH model, (h-k) DP model, and (l) QTM model. DCE, dynamic contrast-enhanced; EXTOFTS, Extended Tofts; ATH, adiabatic tissue homogeneity; DP, distributed parameter; QTM, quantitative transport mapping.

Supplementary Files

This is a list of supplementary files associated with this preprint. Click to download.

- Additionalfile.docx